Forest Height Inversion by Convolutional Neural Networks Based on L-Band PolInSAR Data Without Prior Knowledge Dependency

Dandan Li, Hailiang Lu, Chao Li, Linda Mohaisen, and Weipeng Jing, *Member, IEEE*

***Abstract*—Forest height is a key forest parameter which is of great significance for monitoring forest resources, calculating forest biomass, and observing the global carbon cycle. Because the PolInSAR system could provide various object information including height, shape and direction sensitivity, and spatial distribution, it becomes a powerful means for measuring forest height. The proposed framework utilizes deep learning and builds upon traditional DEM differencing and coherence amplitude inversion algorithms. By using L band PolInSAR data, a new convolutional neural network (CNN) model is established in which the estimated results of DEM differencing and coherence amplitude inversion are used as labels. Furthermore, the PCGrad optimization strategy is used for updating the gradient automatically in the training stage. This model could not only build a relationship between complex coherence and forest height but also makes full use of the spatial context information by using the CNN layers. Experiments are carried out based on the simulated data and real data, named Lope forest site, which are collected by uninhabited aerial vehicle synthetic aperture radar in the NASA AfriSAR campaign. Compared to the classic forest height inversion algorithms, the proposed framework has achieved a higher level of accuracy and performance on RMSE (10.15 m) and R^2 (0.87). Overall, the proposed framework does not require LiDAR data as prior knowledge and can be performed on various forest scenes. Consequently, it will hopefully serve as a useful approach for improvements in forest height inversion based on PolInSAR data.**

***Index Terms*—Artificial intelligence, forestry, neural networks, polarimetry, synthetic aperture radar (SAR).**

I. Introduction

THE forest is the largest terrestrial ecosystem on Earth and is closely related to the carbon cycle, biomass stocks, and global environmental changes [1], [2], [3], [4]. Forest height provides a basis for accurately measuring above-ground biomass and monitoring forest health, and is one of the important parameters of forest ecosystem [5]. Measuring forest height via in situ approach is highly costly and labor-intensive [6], which cannot meet the needs of forest investigation over large areas [7].

In contrast, remote sensing technologies provide a simple way for the retrieval of forest height at regional or global scales. Satellites and aircraft equipped with light detection and ranging (LiDAR) or/and synthetic aperture radar (SAR) offer high-quality data sources for the estimation of forest vertical structure [8], [9]. Whereas, LiDAR is particularly susceptible to cloud, especially on airborne platforms. Therefore, SAR which has a higher cloud penetration capacity is considered suitable and has been widely adopted in forest height estimation, such as BIOSAR 2008 [10] and the NASA AfriSAR campaign [11].

Furthermore, as depicted in Fig. 1, the short-wavelength (X-band or C-band) represents lower penetration capacity than the long-wavelength (L-band) in SAR systems. Forest height retrieval based on short-wavelength can be realized by using interferometric SAR (InSAR) [12] technology combined with a separate digital elevation model (DEM) data [13]. However, such methods require separate reference data and cannot be implemented with a single-frequency sensor.

Polarimetric interferometric SAR (PolInSAR) [14] can separate the scattering phase center among various scattering mechanisms by polarimetry, which is regarded as a promising technology for forest height inversion based on the long-wavelength. It has been widely developed in the past decades [15], [16]. The DEM differencing approach performs forest height retrieval by making the phase difference between canopy and surface phase center [17]. However, the forest height is underestimated because of being affected by forest structure and extinction, which can cause the HV phase center

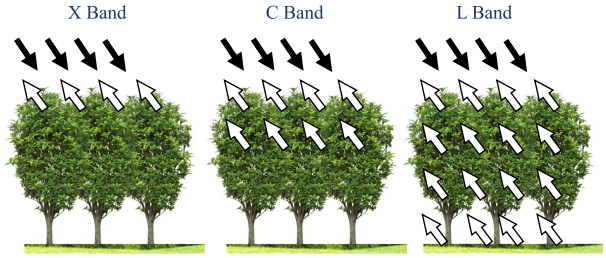

Fig. 1. Diagram of penetration in different bands.

Manuscript received 2 September 2023; revised 3 October 2023; accepted 24 October 2023. Date of publication 30 October 2023; date of current version 23 November 2023. The work was supported by the National Natural Science Foundation of China under Grant 32171777. *(Corresponding authors: Chao Li; Weipeng Jing.)*

Dandan Li, Hailiang Lu, Chao Li, and Weipeng Jing are with the College of Computer and Control Engineering, Northeast Forestry University, Harbin 150040, China (e-mail: dllidandan@nefu.edu.cn; luhailiang@nefu.edu.cn; lichaonefuzyz@nefu.edu.cn; jwp@nefu.edu.cn).

Linda Mohaisen is with the Department of Information Technology, Faculty of Computing and Information Technology, King Abdulaziz University, Jeddah 21589, Saudi Arabia (e-mail: lmohaisen@kau.edu.sa).

Codes, trained model, and data will be available for public access (https://github.com/luhailaing-max/PIDLF).

Digital Object Identifier 10.1109/JSTARS.2023.3328403

not to be at the top but approximately halfway up the volume. As a result, the DEM differencing approach needs to be corrected using prior data [18]. In line with the assumption of a vertically homogeneous volume, the most commonly adopted model for forest height retrieval is the random volume over ground (RVoG) model, which employs an exponential function [19]. Based on the RVoG model, several improvements have been developed. One such improvement is the three-stage algorithm proposed by Cloude [20]. This algorithm breaks down the 6-D optimization process into three separate steps and achieves higher accuracy compared to the DEM differencing approach. To overcome the effects of temporal decorrelation, the RVoG with volume temporal decorrelation model [21] has been developed. The S-RVoG [22] was designed to tackle the errors caused by the slope of the land surface. Fu et al. [23] modified the RVoG model by taking advantage of the heterogeneous vertical structure reflected by the vertically varying extinction coefficient curves of the forest volume layer. Zhang et al. [24] studied a modified two-step approach to the three-stage inversion. Wang et al. [25] studied the influence of different multilooking sizes on forest height inversion based on the RVoG model. Particularly, based on the hypothesis that the extinction coefficient is zero and ignoring the surface phase, the RVoG model was greatly simplified to the sinc function and can be applied to single-polarized data (even a short-wavelength), known as the coherent amplitude inversion [17], [26]. However, the coherent amplitude inversion can result in the overestimation of forest heights due to the temporal decorrelation and signal-to-noise decorrelation [27]. Cloud et al. [17] performed a hybrid algorithm that combined the coherence amplitude and DEM differencing approach to obtain a better estimation than the two algorithms separately. Nevertheless, the forest height retrieval accuracy is difficult to meet the needs of users. Typical shortages are: 1) pixel-based models cannot capture the spatial context information and represent undesired performance; 2) models are not flexible enough; 3) there is a lack of high-quality or representative models [28]. Possible solutions include employing machine learning or deep learning technologies, such as using convolutional neural networks (CNN) to extract spatial context information.

Machine learning and deep learning, which have successful applications in remote sensing, are now gradually gaining attention in SAR research [29], [30]. In the forest height retrieval, Olesk et al. [31] introduced a linear model instead of the sinc function in coherence amplitude inversion and estimate forest height by using signal-polarisation data and LiDAR-derived forest height. Sun et al. [32] proposed a novel inversion strategy to obtain the extinction coefficient by random forest regression. In addition, support vector machine (SVM), which is the most popular and widely adopted machine learning method, has also been introduced to forest height retrieval combined SAR and LiDAR data [33], [34], [35]. Compared with pixel-based traditional methods, the CNN can better capture spatial context information and has been presented for forest height inversion in recent years. For instance, Zhang et al. [36] referred to the low-resolution LiDAR height and proposed an unsupervised generative adversarial network (PolGAN) based on the CNN layer. In addition, they formulated the forest height inversion process as a pan-sharpening procedure, resulting in improved accuracy compared to traditional methods. Furthermore, Ge et al. [28] proposed an improved semisupervised U-Net architecture based on CNN layer, which can be trained without labels but still requires LiDAR data as the prior data. While these methods achieve higher accuracy in forest height estimation, they rely on the availability of corresponding LiDAR data as labels or prior knowledge. However, LiDAR data acquisition is costly and requires microwave expertise to extract forest height map. Moreover, models trained on one forest scene often struggle to achieve similar performance on other scenes.

To address the aforementioned issues, we have developed a CNN-based forest height inversion framework based on full quad-pol L-band SAR data. The proposed framework adopts forest heights underestimated by DEM differencing and overestimated by coherence amplitude inversion as labels for model training. It can be trained and used to predict forest heights for any selected forest scene. The main contributions of this article are summarized as follows.

1) A novel deep learning-based framework for forest height inversion, which combines the DEM differencing and coherence amplitude inversion, has been developed. The proposed framework does not require LiDAR data as labels or prior data. This framework is general and can be used for any deep learning-based model.
2) To effectively obtain the spatial context information, we construct a three-CNN-layer-based model for the proposed framework. This model is designed to map the relationship between forest height and three (HH, HV, VV) complex coherences.
3) To fully exploit the actual height information provided by two labels, a suitable two-component loss is employed. In addition, we introduce an innovative gradient optimization method derived from multitask learning to automatically balance the losses of each component. Experimental results demonstrate the significant potential of gradient optimization within the proposed framework.
4) Experiments are conducted on both simulated data and real data. First, the effectiveness of the proposed framework is verified on simulated data by comparing it with the DEM differencing and coherence amplitude inversion method. Second, the designed framework is integrated into the Kapok software, and its performance is compared with four classic methods, including RVoG, by using real data. The experimental results demonstrate that our proposed framework achieves higher prediction accuracy.

The rest of this article is organized as follows. In Section II, the proposed framework is introduced according to five aspects: 1) overall architecture, 2) DEM differencing, 3) coherence amplitude inversion, 4) CNN model, and 5) PCGrad optimization strategy. Section III describes the experimental data used in this article and introduces the implementation details of the proposed framework. Section IV compares the performance of our framework with four classic forest height inversion algorithms based on the simulated data and real data. Finally, Section V concludes this article.

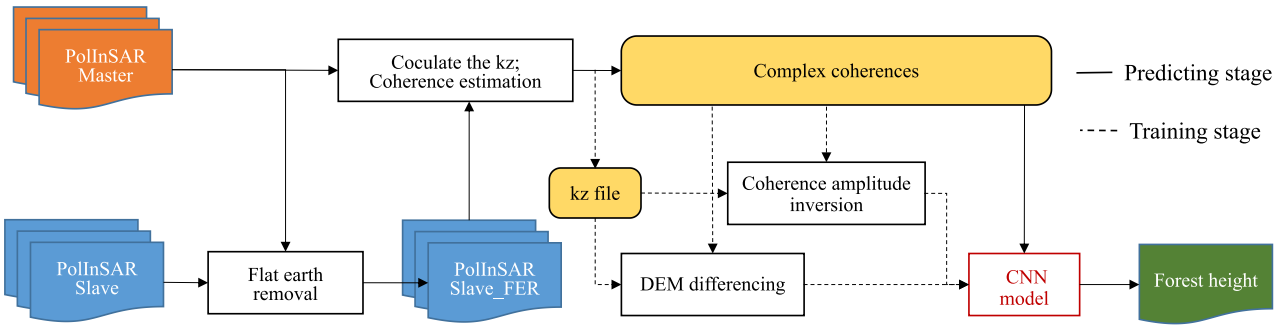

Fig. 2. Concept map of our proposed framework.

II. Proposed Framework

A. Overall Framework

The flowchart of the proposed framework is shown in Fig. 2. It should be noted that the master and slave in Fig. 2 refer to finely calibrated single look complex (SLC) data files, including HH, HV, and VV channels, with calibration done for both radiometry and polarimetry. The "Flat Earth removal" step is necessary because it can remove the negative influence of the background phase variations on the forest height estimation to ensure the performance of the inversion algorithm. Then, the vertical effective wavenumber k_z and complex coherence need to be calculated for the height estimation of the forest by different appendices.

Compared with other methods, the DEM difference and coherent amplitude inversion method are simple and easy to implement. Their inversion results is obviously distributed at two sides of the real forest height (one side is underestimation, the other side is overestimation). This is conducive to the proposed framework to achieve the compromise goal and obtain inversion results closer to the real forest height. Therefore, from the CNN model training stage, the forest height estimated by DEM differencing and coherence amplitude inversion was taken as the labels. In the test stage, the CNN model only needs to predict the corresponding forest height according to the input complex coherences. Therefore, the designed CNN model avoids the influence of variables, such as k_z and the extinction coefficient on forest height prediction by directly establishing a mapping relationship between complex coherences and forest height.

B. DEM Differencing

In the proposed framework, the DEM differencing method selects the corresponding two-phase center: one with a phase center close to the surface (HH-VV) and the other with a phase center close to the top of vegetation canopy (HV), and can be formulated as follows:

$$h_{\text{DEM\_diff}} = \frac{\phi_{HV} - \phi_{HH-VV}}{k_z} = \frac{\arg(\gamma_{w_{HV}}) - \arg(\gamma_{w_{HH-VV}})}{k_z} \tag{1}$$

where ϕ_{HV} represents the vegetation canopy phase, and the ϕ_{HH-VV} denotes the surface phase. $\gamma_{w_{HV}}$ is the corresponding volume coherence, and $\gamma_{w_{HH-VV}}$ is the surface coherence. k_z is the vertical effective wavenumber and can be expressed as

$$k_z = \frac{4\pi\Delta\theta}{\lambda \sin\theta} \approx \frac{4\pi B_\perp}{\lambda R \sin\theta} \tag{2}$$

$$\Delta\theta = \tan^{-1}\left(\tan\theta + \frac{B}{H}\right) - \theta \tag{3}$$

where the θ is the incidence angle of an SAR satellite, and the $\Delta\theta$ is the angular separation of the baseline endpoints from the surface pixel. B denotes the spatial baseline which represents the spatial distance between the master and slave acquisition sites. H is the platform altitude. λ denotes the wavelength. $B_\perp$ represents the vertical baseline, and the R is the distance between the radar antenna and the target.

C. Coherence Amplitude Inversion

The coherence amplitude inversion is the simplified version of RVoG. The formulation from RVoG to the coherence amplitude inversion is given as follows.

The complex interferometric coherence $\gamma(\omega)$ in RVoG can be represented as a normalized sum of the volume coherence γ_v with the ratio of the ground-to-volume amplitude in a polarization channel (ω)

$$\gamma(\omega) = e^{j\varphi_0}\frac{\gamma_v + m(\omega)}{1 + m(\omega)} \tag{4}$$

$$\gamma_v = \frac{p(e^{p_1 h_v} - 1)}{p_1(e^{p h_v} - 1)} \tag{5}$$

$$p = \frac{2\sigma}{\cos\theta_0}, p1 = \frac{2\sigma}{\cos\theta_0} + ik_z \tag{6}$$

where φ_0 denotes the surface phase.

And according to (5) and (6), we can know that the volume coherence γ_v is only related to the vegetation height h_v and extinction σ. If we set $\sigma = 0$, then

$$\gamma_v = e^{\frac{jk_z h_v}{2}} \sin c\left(\frac{k_z h_v}{2}\right). \tag{7}$$

Consequently, the relationship between the forest canopy height and the "pure" volume coherence can be expressed by the sinc

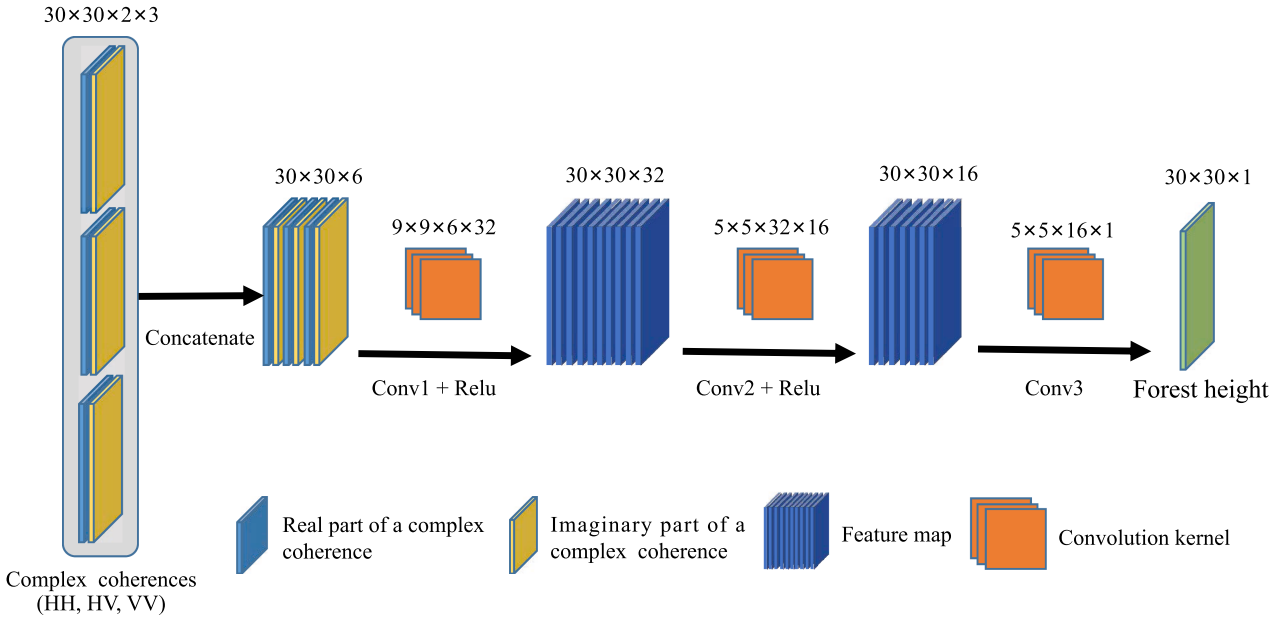

Fig. 3. Architecture of the proposed CNN model.

function (known as the coherence amplitude inversion)

$$\gamma(\omega) = e^{j\varphi_0} e^{\frac{jk_z h_v}{2}} \sin c\left(\frac{k_z h_v}{2}\right) \tag{8}$$

$$|\gamma(\omega)| = \sin c\left(\frac{k_z h_v}{2}\right) \tag{9}$$

$$h_{\text{Sinc}} = \frac{2\arcsin c(|\gamma(\omega)|).}{k_z} \tag{10}$$

D. CNN Model

CNN is designed based on the principles of biological visual perception allowing it to perform both supervised and unsupervised learning. The utilization of parameter sharing in the hidden layer's convolutional kernels and the sparsity of interlayer connections enable the CNN to efficiently process grid-like topology features with minimal computational resources. This approach achieves stable performance in different learning tasks without the need for additional feature engineering on the given data [37]. Therefore, it has received significant attention in pixel-level regression tasks, such as spatiotemporal image fusion [38], which has inspired the design of our CNN model.

Unlike the typical CNN structure, we removed the pooling layer to maintain the image size unchanged during the feature extraction process. In addition, the fully connected layer was also ignored. As a result, the proposed CNN model primarily consists of the CNN layer and activation layer. Suppose we have the input X with the size of $H \times W \times C$, where H, W, and C represent the height, width, and number of channels, respectively. The output of a CNN layer can be formulated as follows [39]:

$$\mathrm{Z}_j = \sum_{i=1}^{C} \mathrm{X}_i * \mathrm{W}_j + \mathrm{B}_j, j = 1, 2, 3, \ldots, k \tag{11}$$

where i represents the ith channel, j denotes the jth filter, and the k is the total number of filters. The W and B are the parameters that need to be learned in the model training process. Z represents the output of a CNN layer. The discrete convolution operation is denoted by $*$.

For enhancing the nonlinear fitting ability of the CNN model and avoiding gradient disappearance, the rectified linear unit (ReLU) [40] is adopted after each CNN layer except the last layer. The activation layer (ReLU $\xi(\cdot)$) can be denoted as

$$\xi(x) = \max(0, x) = \begin{cases} 0 & \text{if } x < 0 \\ x & \text{if } x \geq 0 \end{cases} \tag{12}$$

where x is an element from Z.

The overall structure of the designed CNN model is shown in Fig. 3. It consists of three convolutional layers and two activation layers. In the definition of the convolutional layer, an appropriate padding value is chosen to maintain the size of the extracted feature map consistent with the size of the input. Theoretically, appropriate convolution kernel sizes should be used for different scenes to ensure the extraction of optimal features. For instance, small size (3×3) convolution kernels can be used for planted areas [41]. Compared with crops, the spatial variation of forest canopy is much more severe between tree stands. Therefore, larger convolution kernels are used in forest areas to ensure a large receptive field and capture sufficient spatial information [36]. Consequently, in the CNN model, the first convolutional layer has a convolution kernel size of 9×9 with a padding of length 4, while the other two have a convolution kernel size of 5×5 with a padding of length 2. The model first concatenates the input complex coherences (HH, HV, VV) in the channel dimension. Then, the last convolutional layer is responsible for predicting the corresponding forest height.

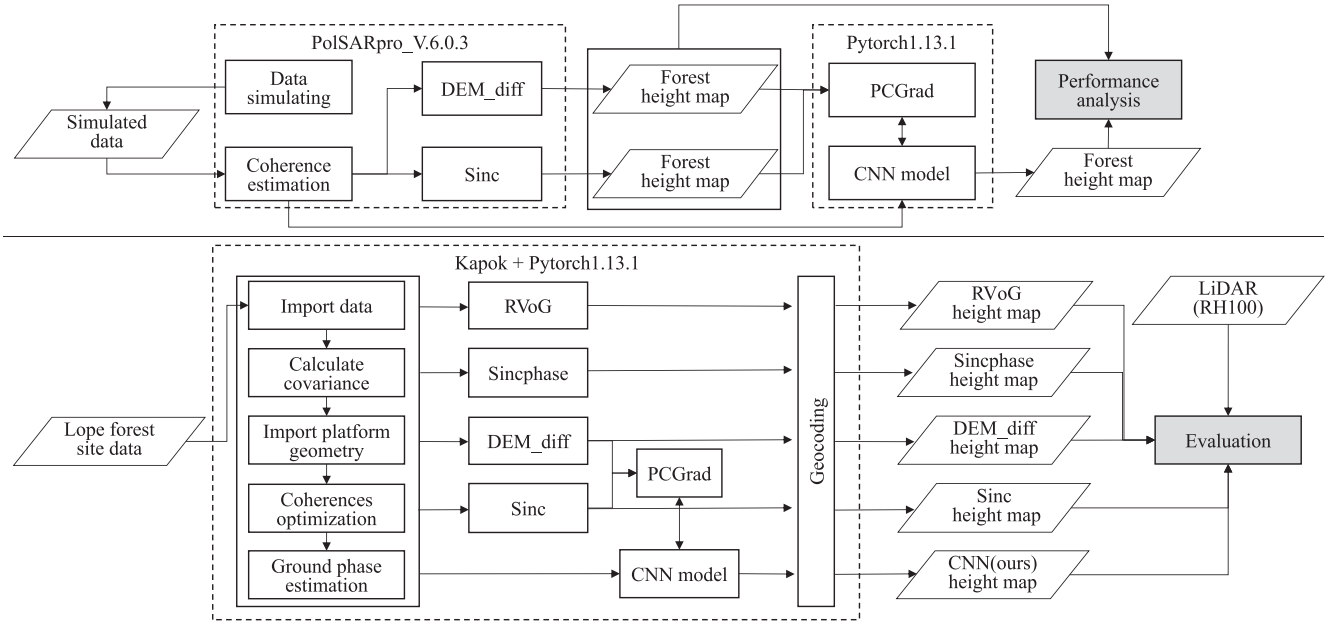

Fig. 4. Experimental technology roadmap on simulated data and real data, respectively.

E. PCGrad Optimization Strategy

The constructed CNN model utilizes the forest height underestimated by DEM differencing ($h_{\text{DEM\_diff}}$) and overestimated by coherence amplitude inversion (h_{Sinc}) as guidance. To fully explore the forest height information present in the two labels, a two-component loss function was developed. To evaluate the contribution of the two components to the loss function, we adopted the PyTorch version [42] of the projecting conflicting gradients (PCGrad) [43] optimization strategy. This strategy, derived from multitask learning, automatically balances the losses of each component.

The mean square error (mse)-based loss function was adopted for the two components

$$\mathcal{L}_1 = \text{MSE}(h_{\text{DEM\_diff}}, \text{Y}) \tag{13}$$

$$\mathcal{L}_2 = \text{MSE}(h_{\text{Sinc}}, \text{Y}) \tag{14}$$

where Y presents the forest height predicted by the CNN model. Then, for model parameter θ, the gradient of $\mathcal{L}_1$ can be denoted as $g_1 = \nabla\mathcal{L}_1(\theta)$, and the gradient of $\mathcal{L}_2$ can be denoted as $g_2 = \nabla\mathcal{L}_2(\theta)$. The total gradient is $g = g_1 + g_2$. The corresponding dual-task optimization objective can be defined as

$$\mathcal{L} = \mathcal{L}_1(\theta) + \mathcal{L}_2(\theta) \tag{15}$$

$$g_1 = g_1 - \frac{g_1 \cdot g_2}{\|g_2\|^2} g_2. \tag{16}$$

The optimization of PCGrad for the objective above are as follows. First, the cosine similarity is used to calculate the similarity between g_1 and g_2. If the result is negative, the two gradients are considered to be in conflict. Second, when the gradients are conflicted, the g_1 will be replaced by its projection onto the normal plane of g_2 through (16). If the cosine similarity is positive, which indicates that there is no conflict between gradients, then the gradient of g_1 remains unchanged. Finally, by optimizing the gradient of PCGrad, we can make the CNN model's prediction increasingly accurate in estimating forest height.

III. Experimental Setup

In the experiments, we first validate the effectiveness of the proposed framework using simulated data. Then, we verify the advancements of the proposed framework using real data. The technical route of the experiment is shown in Fig. 4.

A. Dataset

Simulated Data: With the development of the 3-D coherent SAR simulator [44], scholars only need to focus on algorithm design. Therefore, simulated PolInSAR data has been widely adopted in forest height estimation [20], [17], [45]. PolSARpro [46] is an open-source PolInSAR data processing software developed by the European Space Agency (ESA). It also integrates the SAR simulator tool, providing an ideal data basis. Therefore, the PolSARpro-SIM tool of PolSARpr_V.6.0.3 is adopted to simulate the Pineland data, which is the fully polarized single-baseline L-band data. The main parameters for simulating can be found in Table I.

Real Data: The real data used in this article were collected by uninhabited aerial vehicle synthetic aperture radar (UAVSAR), which is an airborne equipped with a platform precision autopilot (PPA) and a fully polarimetric L-band SAR system (1.26 GHz, 80-MHz bandwidth). The data were collected on 25 February 2016 in Gabon, West Africa, specifically at the Lope forest site, as part of the NASA AfriSAR campaign [47]. The data are publicly available on the UAVSAR website.[1] This site is suitable for evaluating forest height inversion as it comprises extensive areas of tropical forests with comprehensive data

[1][Online]. Available: uavsar.jpl.nasa.gov

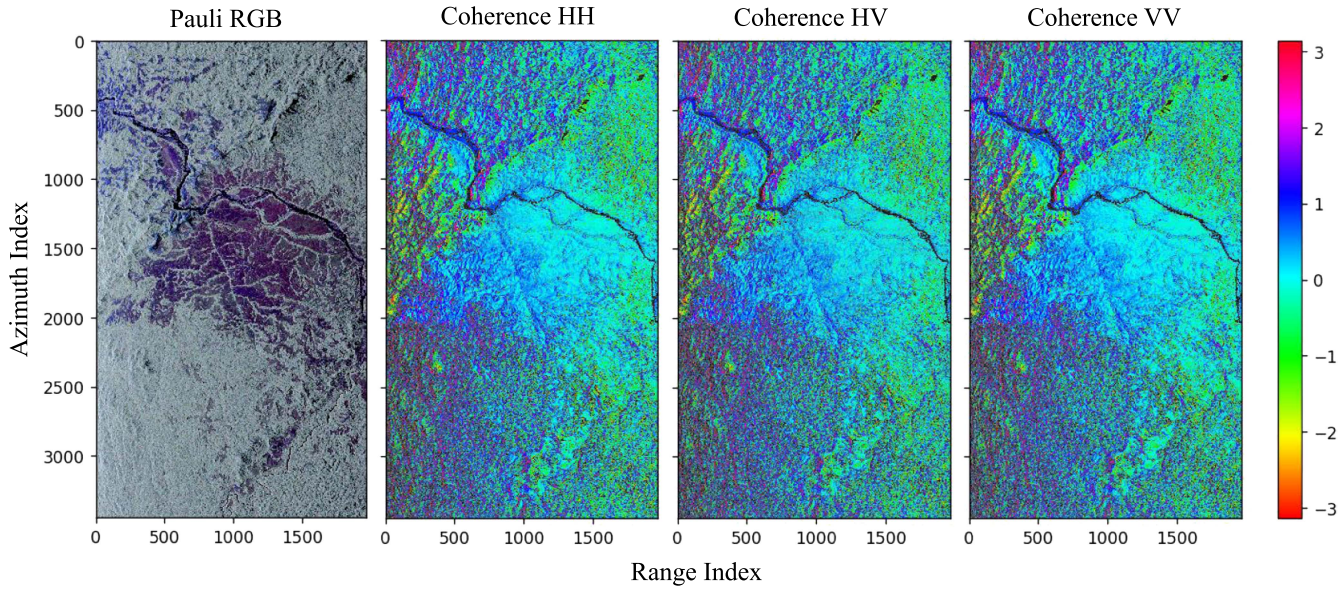

Fig. 5. Visualization of the Lope forest site in Pauli RGB and coherences (HH, HV, VV).

TABLE I
PARAMETERS ADOPTED FOR THE PINELAND SIMULATION OF 18 M

Simulator parameters	Value	Unit
Platform Altitude	3000	Meter
Horizontal Baseline	10	Meter
Incidence Angle	45	Degree
Vertical Baseline	1	Meter
Center Frequency	1.3	G Hertz
Azimuth Resolution	1.5	Meter
Azimuth Ground Slope	2.0	%
Slant Range Resolution	1.06066	Meter
Tree Species	1	Pine
Range Ground Slope	1	%
Forest Stand Circular Area	0.282745	Hectare
Tree Height	18.0	Meter
Forest Stand Density	300	stems/Hectare

description documentation. An illustration of the Lope forest site is presented in Fig. 5. In addition, NASA's airborne land, vegetation, and ice sensor (LVIS) provides an accurate forest vertical structure by digitally recording the signals reflected by the laser. It is commonly used for performance verification of forest height inversion algorithms based on SAR data. Therefore, the gridded forest height products (RH100) with a 25-m resolution [48], derived from full-waveform lidar data acquired by LVIS instrument, were selected to be the ground truth.

B. Experimental Settings

We choose four classic algorithms of forest height retrieval to evaluate the performance of the proposed framework as follows.

1) *DEM Differencing (DEM_diff):* This algorithm selects two interferograms, one of which represents the surface phase center, and the other one represents the phase center of the canopy top. Then the forest height map can be obtained by the phase differencing of two interferograms.
2) *Coherence Amplitude Inversion (Sinc):* Ihis algorithm is a simplified version of RVoG. It establishes the relationship between the forest height and the "pure" volume coherence into a sinc function.
3) *Hybrid (Sincphase):* This approach combines the DEM differencing and coherence amplitude inversion methods. The forest height can be obtained by using the coherence amplitude term to compensate for the DEM differencing.
4) *RVoG* [20]*:* The process of 6-D optimization of the full RVoG model is broken down into three separate steps, also known as three-stage inversion.

Due to the absence of labels in the simulated data for quantitative evaluation, comparison of more methods would create difficulties in demonstrating the effectiveness of the proposed framework. Therefore, we only conduct a comparative analysis of the proposed framework with two related traditional methods (DEM_diff, Sinc) to clearly demonstrate the compromise effect of the proposed framework. With real data, we integrate the proposed framework into Kapok [49] software package, which is an open-source Python library developed for forest height inversion using the UAVSAR data format. The four methods mentioned above were compared with the proposed framework to show the advancement. In addition, for both simulated and real forest scenes, we cropped the complex coherences into blocks with $30 \times 30 \times 6$ pixels in which 30×30 represents the height and width, and 6 is the number of channels which was obtained by concatenating all input complex coherences. The proposed framework aims to reduce the computation cost of the CNN model by limiting the input data. Therefore, three complex coherences (HH, HV, VV) based on the linear

polarization basis were selected to be the CNN model inputs in experiments. PyTorch 1.13.1 was used to construct the CNN model of the proposed framework. The SGD optimizer with the initial learning rate of 0.0001 is adopted, and the weight decay is set to 0.000001. Eventually, the trained model was obtained after 10 000 epochs.

C. Quantitative Evaluation

Quantitative evaluation is to use mathematical statistics methods to calculate the physical characteristic values between the inversion results and the real forest height. By reflecting the quality of the inversion results through quantitative evaluation, the performance of the inversion methods can be achieved. Five indicators were selected for accuracy evaluation in the experiment. The formulas for each indicator are as follows:

$$\mathrm{RMSE} = \sqrt{\frac{\sum_{i=1}^{n}(Y_i - \widehat{Y}_i)^2}{n}} \tag{17}$$

$$\mathrm{MAE} = \frac{\sum_{i=1}^{n}|Y_i - \widehat{Y}_i|}{n} \tag{18}$$

$$\mathrm{R}^2 = 1 - \frac{\sum_{i=1}^{n}(Y_i - \widehat{Y}_i)^2}{\sum_{i=1}^{n}(Y_i - \overline{Y}_i)^2} \tag{19}$$

$$\mathrm{RMSE\%} = \frac{\mathrm{RMSE}}{\overline{Y}} \cdot 100\% \tag{20}$$

$$\mathrm{BIAS} = \frac{\sum_{i=1}^{n}(\widehat{Y}_i - Y_i)}{n} \tag{21}$$

where $\widehat{Y}_i$ and Y_i are inversion results and reference forest height map, respectively. $\overline{Y}$ is the average height. And n represents the number of pixels.

IV. Results and Discussion

The proposed framework adopts the forest height maps derived from DEM differencing and coherence amplitude inversion as labels for training. The real forest height information hidden in these forest height maps can be fully explored by the CNN model to improve the inversion accuracy. The validity and advancement of the proposed framework are verified based on simulated data and real data, respectively.

A. Experiment on Simulating Data

The different heights of Pineland were simulated by PolSARpro_V.6.0.3, including 6, 10, 12, 14, 16, 18, 19, 20, and 23 m. Among them, 6, 12, 16, 18, 20, and 23 m were used for model training, and 10, 14, and 19 m were used for evaluation.

As shown in Table I, the tree species used for the simulation data in the experiment is pine (Tree Species = 1). The forest stand density is 300 stems/hectare, and the simulated forest stand circular area is 0.282745 hectares, which corresponds to approximately 84 simulated pines. Each pine occupies approximately 33.33 m^2, which contains several pixels. Therefore, due to the canopy characteristics of pine and large tree spacing, it can be determined that the average forest height corresponding to all pixels in the forest range should be less than the simulated tree height. In addition, it is not difficult to determine that the maximum height in the forest area should be the simulated height, and a lot of pixels in the forest region have a lower height than the simulated height.

TABLE II
Comparison of Mean, Maximum and Minimum of Forest Height Inversion by DEM Differencing (DEM_diff), Coherence Amplitude Inversion (Sinc) and the Proposed Framework (PIDLF)

	Max (m)	Min (m)	Mean (m)
10m			
DEM_diff	7.00	1.00	1.75
Sinc	24.00	3.00	11.17
PIDLF (ours)	13.00	2.00	7.02
14m			
DEM_diff	11.00	1.00	2.47
Sinc	32.00	4.00	14.83
PIDLF (ours)	21.00	1.00	8.97
19m			
DEM_diff	14.00	1.00	3.10
Sinc	49.00	7.00	18.22
PIDLF (ours)	30.00	1.00	10.77

Based on the analysis, we calculated the mean, maximum, and minimum pixel values for the forest region in Table II, which shows the estimated forest height using all methods. The DEM differencing (DEM_diff) shows the lowest mean on all test data, and the coherence amplitude inversion (Sinc) shows an obvious overestimation on 10 and 14-m test data. This observation is consistent with the conclusion obtained in [17]. Furthermore, the mean height obtained by the proposed framework, named polarimetric interferometric deep learning-based framework (PIDLF), is more reasonable.

It is difficult to distinguish whether Sinc overestimates the mean height, as it shows the same height as the simulation. However, the mean height of the forest area can be significantly lower than the simulated height due to the presence of ground among the trees. Meanwhile, DEM_diff still shows underestimation, while PIDLF shows overestimation, but the overestimation is significantly improved compared to Sinc. The minimum height represents the ground height, which tends to be 0 m in principle. However, due to the backscatter from different objects, such as the volume scatter of nearby trees, the corresponding surface pixels will also have a higher backscatter. Therefore, a certain height value will also be presented in the inversion results. In all test data, the PIDLF can achieve a good compromise, while the DEM_diff prediction is the closest to the real ground.

To further reflect the performance of the proposed framework, the position of 40 on the azimuth dimension is selected to show transects of all test data along the range dimension. As shown in Fig. 6, the horizontal axis represents the range dimension of simulated images and the vertical axis represents the canopy height. For the DEM_diff, all pixels on the transects are underestimated, and a large number of pixels in the Sinc are

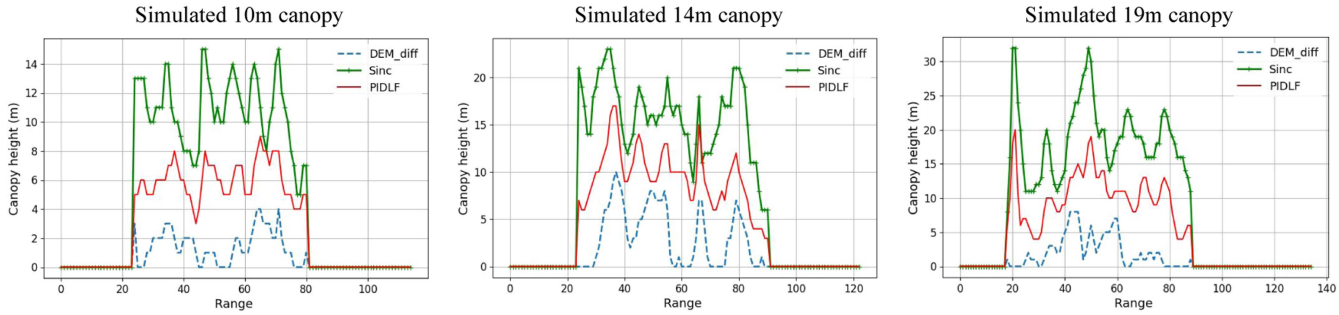

Fig. 6. Range transects through the height profiles for the position of azimuth = 40.

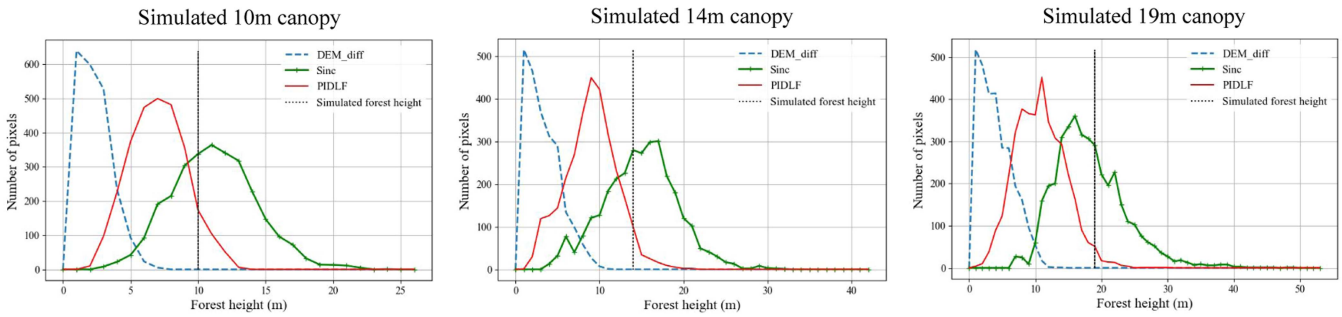

Fig. 7. Statistics of all forest height values in forest region.

overestimated. However, the PIDLF in this article can achieve a good compromise. By referring to the forest height estimation through DEM_diff and Sinc, the true forest height information is fully mined. Furthermore, the PIDLF can obtain the estimated results closer to the real forest height. In addition, Fig. 7 shows the distribution of the estimated height from all methods in terms of the number of pixels. The horizontal axis represents the estimated forest height, and the vertical axis represents the total number of pixels at a certain height. From the previous analysis, we can know that the maximum height of the inversion should not exceed the simulated height. Therefore, for the Sinc method, there are a large number of pixels to the right of the simulated forest height, which is overestimated. All pixel distributions in the DEM_diff method are far away from the simulated height to the left, which shows an obvious underestimation. The PIDLF also shows underestimation, but the overall estimation is more reasonable.

B. Experiment on Real Data

In this section, the four previously mentioned algorithms and the proposed framework were applied to estimate forest height over the Lope forest site. The Lope forest site is located in the center area of Gabon and mainly consists of well-preserved tropical rainforest and grassland habitat. Mature forest heights range from 30 to 50 m [50]. The original SLC product of the Lope forest site has a 1-m resolution in azimuth and 2.5-m resolution within ground range [51]. The temporal baseline is 23 min, and the vertical baseline is 20 m. For the evaluation, the RH100 forest height product (Fig. 8) is used, which is derived from LVIS and gridded by Armston et al. [48].

During our experiments, the Kapok software first imported the SLC product and processed it into an HDF5 format file by using the multilook window (20, 5), where the first index represents the azimuth size and the second index is the range size. Then, the forest height map can be estimated by different algorithms. Fig. 8 illustrates the estimation of the forest height map over the Lope forest site by five algorithms. The forest height was uniformly set within the range of 0–100 m. The RH100 forest height map does not cover the whole Lope forest site, and some pixels were set as NoData due to the absence of the LVIS LiDAR acquisitions. Meanwhile, referring to the maximum height of 63.91 m in RH100, there is a large number of pixels tending to be yellow in Sinc and Sincphase, indicating a serious overestimation, while the DEM_diff shows a significant underestimation. From the viewing of estimated forest height maps, the proposed framework (PIDLF) exhibits similar color and texture to RVoG. It is necessary to further evaluate it by using quantitative evaluation metrics to certify its advancement.

Comparisons of the four algorithms with the proposed framework (PIDLF) were presented in Table III. Based on the area covered by RH100, the height maps retrieved by each method are aligned to the resolution of RH100, which is at 25 × 25 m/pixel, using the nearest neighbor interpolation. From the overall results in Table III, the DEM differencing (DEM_diff) exhibits the worst performance, obtaining 17.19 m at RMSE, 14.64 m at MAE, 1.69 at R^2, 1.92 at RMSE%, and −12.72 m at BIAS. The coherence amplitude inversion (Sinc) performs better than DEM_diff and

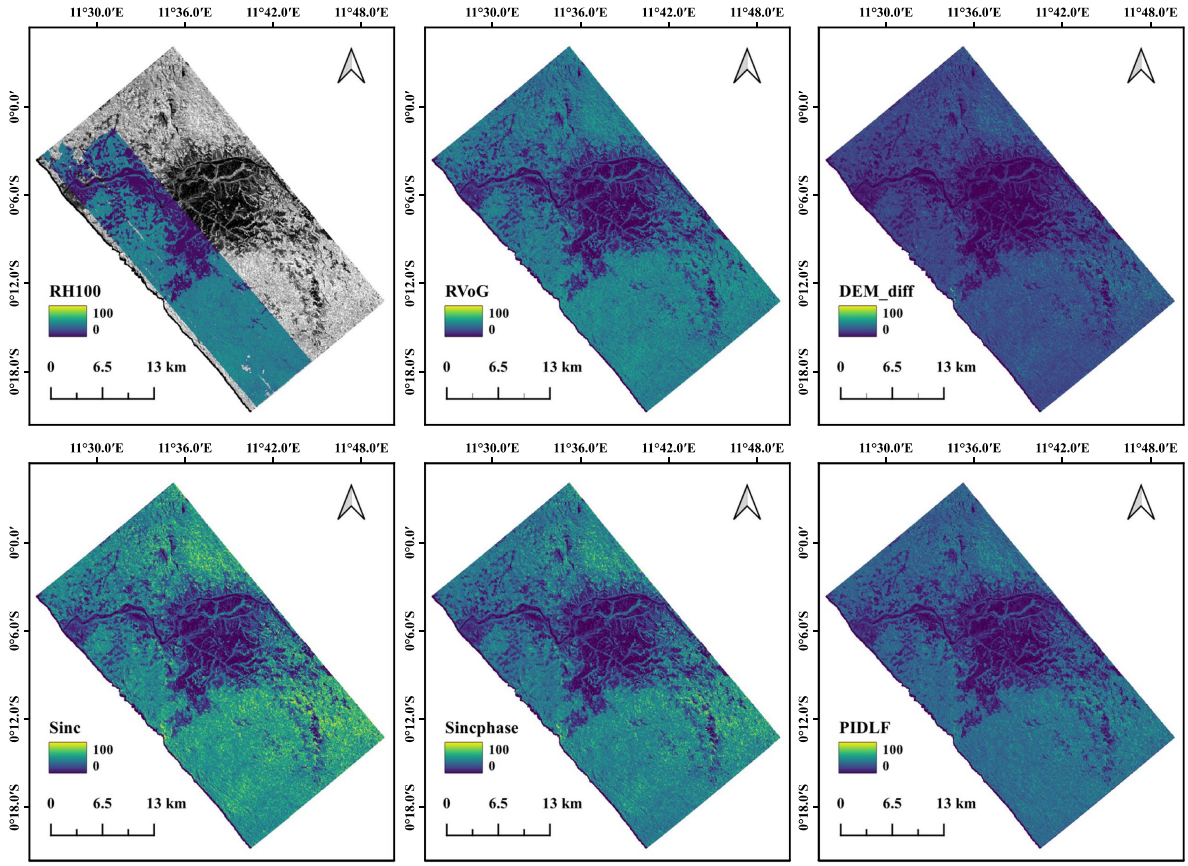

Fig. 8. Ground truth and the map of forest height by different algorithms: RH100 is the ground truth; The RVoG model was implemented by using the three-stage inversion; DEM_diff is the DEM differencing algorithm; Sinc presents the coherence amplitude inversion; Sincphase is the fusion of DEM_diff and Sinc; PIDLF (ours) is the proposed Polarimetric Interferometric Deep Learning-based Framework.

TABLE III
QUANTITATIVE EVALUATION IN RMSE, MAE, R^2, RMSE%, AND BIAS FOR ALL INVERSION METHODS

	RMSE (m) ↓	MAE (m) ↓	R^2 ↑	RMSE% ↓	BIAS (m)
DEM_diff	17.19	14.64	0.69	1.92	-12.72
Sinc	15.65	12.31	0.71	1.75	10.08
Sincphase	11.58	8.82	0.83	1.29	3.66
RVoG	10.35	8.07	0.86	1.15	3.14
PIDLF (ours)	10.15	8.13	0.87	1.13	-3.13

has achieved 15.65 m at RMSE, 12.31 m at MAE, 0.71 at R^2, 1.75 at RMSE%, and 10.08 m at BIAS. For the hybrid Sincphase, which is a fusion of DEM_diff and Sinc, the performance has been greatly improved but is still inferior to RVoG which has 10.35 m at RMSE, 8.07 m at MAE, 0.86 at R^2, 1.15 at RMSE%, and 3.14 m at BIAS. However, the PIDLF can obtain better estimation accuracy and has achieved 10.15 m at RMSE, 8.13 m at MAE, 0.87 at R^2, 1.13 at RMSE%, and -3.13 m at BIAS. Only at MAE, the RVoG performed slightly better than PIDLE.

C. Validity of PCGrad

To further demonstrate the performance of the PCGrad optimization in the proposed framework, we perform extra comparisons among four loss strategies (Table IV) as follows.

1) Using height map from DEM_diff as label.
2) Using height map from Sinc as label.
3) Using height map from Sincphase (DEM_diff $+ 0.4 *$ Sinc) as label.
4) Using height maps from DEM_diff and Sinc as label and the PCGrad optimization.

To achieve a fair comparison, all the experimental parameters remain the same.

Table IV shows the comparisons among four loss strategies. Using DEM as a label, the RMSE is larger and the BIAS is -11.74 m, showing a larger underestimation. When the label is changed to Sinc, the RMSE is reduced, but obtained 9 m at BIAS, which shows an obvious overestimation. The Sincphase which is a hybrid of DEM_diff and Sinc, can obtain better inversion results. But training as labels in our proposed framework shows

TABLE IV
PERFORMANCE UNDER DIFFERENT LOSS STRATEGIES AND DIFFERENT LABELS

	Label		Loss Strategy		RMSE (m) ↓	MAE (m) ↓	R^2 ↑	RMSE% ↓	BIAS (m)
	DEM_diff	**Sinc**	**MSE**	**PCGrad**					
PIDLF	√	×	√	×	16.08	13.69	0.73	1.79	-11.74
	×	√	√	×	13.58	10.92	0.77	1.51	9.00
	√	√	√	×	20.92	17.82	0.51	2.33	17.07
	√	√	√	√	10.15	8.13	0.87	1.13	-3.13

the worst results. The main reason for this is that our proposed framework further amplifies this overestimation trend during the learning process. By using both DEM_diff and Sinc as labels, the proposed framework with PCGrad optimization outperforms others and generates more accurate results.

D. Discussion

This article has presented a theoretical and experimental study on the forest height inversion process. A deep learning-based framework is proposed to effectively extract the true forest height information from the height maps estimated by DEM differencing and coherence amplitude inversion. In general, the proposed framework provides an alternative direction for current forest height retrieval based on PolInSAR data.

Both simulated data and real data are adopted in the experiments. First, the effectiveness of the proposed framework is verified with simulated data compared with DEM differencing and coherence amplitude inversion. Based on the estimated forest height maps, statistics and analysis are carried out, demonstrating that the proposed framework can achieve a clear tradeoff between DEM differencing and coherence amplitude inversion. When comparing the proposed framework to the previous algorithms, including RVoG, on real data, the proposed framework achieves an RMSE of 10.15 m, outperforming RVoG by approximately 0.2 m. In addition, the R^2 of the proposed framework is increased to 0.87, compared to 0.86 for RVoG. Although RVoG is lower than the proposed framework on MAE. But on the other two indicators (RMSE%, BIAS), the proposed framework also showed better results. Therefore, the proposed framework can better estimate the forest height without the need for a complex modeling procedure.

However, the inversion accuracy of the proposed framework is still inadequate, and additional computational cost is required for model training. Despite its limitation, this article does provide a new idea for forest height retrieval. Furthermore, we have only implemented the simplest version of the proposed framework. We believe that there is still a lot of room for expansion and further improvement. Future research directions include applying more efficient deep learning models or using more complex coherence extracted from PolInSAR data as input.

V. CONCLUSION

In this article, a deep learning-based framework was proposed for forest height retrieval using single-baseline L-band PolInSAR data. To address the shortcoming of current deep learning methods that require the collection of LiDAR data as labels or priors, the proposed framework adopts a CNN structure, uses the inversion results of two traditional methods as labels, and innovatively introduces the PCGrad optimization strategy. Consequently, the proposed framework does not require additional LiDAR data and can be easily applied to any forest scene. The experiments have been conducted on simulated data and real data, both qualitative and quantitative verifications demonstrated that the proposed framework can achieve more accuracy performances compared with several classical algorithms. However, there are some abnormal pixel values in the labels which are produced by two traditional methods. This directly affects the inversion accuracy of our framework. Future works include improving the quality of labels or adopting a more efficient network structure to improve the performance of forest height retrieval.

REFERENCES

[1] Z. Liao, B. He, and Y. Shi, "Improved forest biomass estimation based on P-band repeat-pass POLinSAR data across different forest sites," *Int. J. Appl. Earth Observ. Geoinformation*, vol. 115, 2022, Art. no. 103088.

[2] I. D. S. Narvaes, J. R. D. Santos, P. D. C. Bispo, P. M. D. A. Graça, U. S. Guimarães, and F. F. Gama, "Estimating forest above-ground biomass in central Amazonia using polarimetric attributes of ALOS/PALSAR images," *Forests*, vol. 14, no. 5, 2023, Art. no. 941.

[3] J. Erbaugh et al., "Global forest restoration and the importance of prioritizing local communities," *Nature Ecol. Evol.*, vol. 4, no. 11, pp. 1472–1476, 2020.

[4] P. Potapov et al., "Mapping global forest canopy height through integration of GEDI and Landsat data," *Remote Sens. Environ.*, vol. 253, 2021, Art. no. 112165.

[5] F. Kugler, S.-K. Lee, I. Hajnsek, and K. P. Papathanassiou, "Forest height estimation by means of Pol-inSAR data inversion: The role of the verticalwavenumber," *IEEE Trans. Geosci. Remote Sens.*, vol. 53, no. 10, pp. 5294–5311, Oct. 2015.

[6] X. Liang et al., "In-situ measurements from mobile platforms: An emerging approach to address the old challenges associated with forest inventories," *ISPRS J. Photogrammetry Remote Sens.*, vol. 143, pp. 97–107, 2018.

[7] M. Holopainen, M. Vastaranta, and J. Hyyppä, "Outlook for the next generation's precision forestry in Finland," *Forests*, vol. 5, no. 7, pp. 1682–1694, 2014. [Online]. Available: https://www.mdpi.com/1999-4907/5/7/1682

[8] R. Sa, Y. Nei, and W. Fan, "Combining multi-dimensional SAR parameters to improve RVOG model for coniferous forest height inversion using ALOS-2 data," *Remote Sens.*, vol. 15, no. 5, 2023, Art. no. 1272.

[9] S. Tebaldini et al., "Tomosense: A unique 3D dataset over temperate forest combining multi-frequency mono-and bi-static tomographic SAR with terrestrial, UAV and airborne LiDAR, and in-situ forest census," *Remote Sens. Environ.*, vol. 290, 2023, Art. no. 113532.

[10] I. Hajnsek et al., "BioSAR 2008: Final report," DLR, Cologne, Germany, Tech. Rep. 22052/08/NL/CT-002 Nov. 2009. [Online]. Available: https://elib.dlr.de/63157/

[11] L. Fatoyinbo et al., "The 2016 nasa AfriSAR campaign: Airborne SAR and LiDAR measurements of tropical forest structure and biomass in support of future satellite missions," in *Proc. IEEE Int. Geosci. Remote Sens. Symp.*, 2017, pp. 4286–4287.

[12] A. Rogers and R. Ingalls, "Venus: Mapping the surface reflectivity by radar interferometry," *Science*, vol. 165, no. 3895, pp. 797–799, 1969.
[13] P. Kumar and A. P. Krishna, "InSAR-based tree height estimation of hilly forest using multitemporal radarsat-1 and sentinel-1 SAR data," *IEEE J. Sel. Topics Appl. Earth Observ. Remote Sens.*, vol. 12, no. 12, pp. 5147–5152, 2019.
[14] S. R. Cloude and K. P. Papathanassiou, "Polarimetric SAR interferometry," *IEEE Trans. Geosci. Remote Sens.*, vol. 36, no. 5, pp. 1551–1565, Sep. 1998.
[15] S. Cloude and K. Papathanssiou, "Polarimetric optimisation in radar interferometry," *Electron. Lett.*, vol. 33, no 13, pp. 1176–1178, 1997.
[16] Q. Zhang, S. Hensley, R. Zhang, C. Liu, and L. Ge, "Improved model-based forest height inversion using airborne L-band repeat-pass dual-baseline Pol-InSAR data," *Remote Sens.*, vol. 14, no. 20, 2022, Art. no. 5234.
[17] S. R. Cloude, "Pol-InSAR training course," 2005.
[18] M. J. Soja and L. M. Ulander, "Digital canopy model estimation from tandem-x interferometry using high-resolution LiDAR DEM," in *Proc. IEEE Int. Geosci. Remote Sens. Symp.*, 2013, pp. 165–168.
[19] K. P. Papathanassiou and S. R. Cloude, "Single-baseline polarimetric SAR interferometry," *IEEE Trans. Geosci. Remote Sens.*, vol. 39, no. 11, pp. 2352–2363, Nov. 2001.
[20] S. Cloude and K. Papathanassiou, "Three-stage inversion process for polarimetric SAR interferometry," *IEE Proc.-Radar, Sonar Navigation*, vol. 150, no. 3, pp. 125–134, 2003.
[21] K. P. Papathanassiou and S. R. Cloude, "The effect of temporal decorrelation on the inversion of forest parameters from Pol-InSAR data," in *Proc. Int. Geosci. Remote Sens. Symp.*, 2003, pp. 1429–1431.
[22] H. Lu, Z. Suo, R. Guo, and Z. Bao, "S-RVoG model for forest parameters inversion over underlying topography," *Electron. Lett.*, vol. 49, no. 9, pp. 618–620, 2013.
[23] W. Fu, H. Guo, P. Song, B. Tian, X. Li, and Z. Sun, "Combination of PolInSAR and LiDAR techniques for forest height estimation," *IEEE Geosci. Remote Sens. Lett.*, vol. 14, no. 8, pp. 1218–1222, Aug. 2017.
[24] J. Zhang, Y. Zhang, W. Fan, L. He, Y. Yu, and X. Mao, "A modified two-steps three-stage inversion algorithm for forest height inversion using single-baseline L-band PolInSAR data," *Remote Sens.*, vol. 14, no. 9, 2022, Art. no. 1986.
[25] C. Wang, C. Hu, P. Shen, and T. Song, "Evaluation of multilooking size on single-baseline PolInSAR forest height inversion," *Forests*, vol. 13, no. 7, 2022, Art. no. 1031.
[26] W. Qi and R. O. Dubayah, "Combining tandem-X InSAR and simulated GEDI LiDAR observations for forest structure mapping," *Remote Sens. Environ.*, vol. 187, pp. 253–266, 2016.
[27] H. Luo, B. Zhu, C. Yue, N. Wang, and S. Chen, "Semiempirical compensated optimal coherence amplitude method to invert forest height based on insar," *J. Appl. Remote Sens.*, vol. 16, no. 3, 2022, Art. no. 034533.
[28] S. Ge, H. Gu, W. Su, J. Praks, and O. Antropov, "Improved semisupervised unet deep learning model for forest height mapping with satellite SAR and optical data," *IEEE J. Sel. Topics Appl. Earth Observ. Remote Sens.*, vol. 15, pp. 5776–5787, 2022.
[29] N. Anantrasirichai, J. Biggs, F. Albino, P. Hill, and D. Bull, "Application of machine learning to classification of volcanic deformation in routinely generated InSAR data," *J. Geophysical Res.: Solid Earth*, vol. 123, no. 8, pp. 6592–6606, 2018.
[30] X. X. Zhu et al., "Deep learning meets SAR: Concepts, models, pitfalls, and perspectives," *IEEE Geosci. Remote Sens. Mag.*, vol. 9, no. 4, pp. 143–172, Dec. 2021.
[31] A. Olesk, J. Praks, O. Antropov, K. Zalite, T. Arumäe, and K. Voormansik, "Interferometric SAR coherence models for characterization of hemiboreal forests using tanDEM-X data," *Remote Sens.*, vol. 8, no. 9, 2016, Art. no. 700.
[32] X. Sun, B. Wang, M. Xiang, X. Fu, and S. Jiang, "Machine learning inversion for single-baseline P-band polarimetric SAR interferometry," *IEEE Geosci. Remote Sens. Lett.*, vol. 19, 2021, Art. no. 4000305.
[33] M. García, S. Saatchi, S. Ustin, and H. Balzter, "Modelling forest canopy height by integrating airborne lidar samples with satellite radar and multispectral imagery," *Int. J. Appl. Earth Observ. Geoinformation*, vol. 66, pp. 159–173, 2018.
[34] M. Pourshamsi, M. Garcia, M. Lavalle, and H. Balzter, "A machine-learning approach to PolInSAR and LiDAR data fusion for improved tropical forest canopy height estimation using NASA AfriSAR campaign data," *IEEE J. Sel. Topics Appl. Earth Observ. Remote Sens.*, vol. 11, no. 10, pp. 3453–3463, Oct. 2018.
[35] M. Pourshamsi et al., "Tropical forest canopy height estimation from combined polarimetric SAR and LiDAR using machine-learning," *ISPRS J. Photogrammetry Remote Sens.*, vol. 172, pp. 79–94, 2021.
[36] Q. Zhang, L. Ge, S. Hensley, G. I. Metternicht, C. Liu, and R. Zhang, "Polgan: A deep-learning-based unsupervised forest height estimation based on the synergy of PolInSAR and LiDAR data," *ISPRS J. Photogrammetry Remote Sens.*, vol. 186, pp. 123–139, 2022.
[37] J. Gu et al., "Recent advances in convolutional neural networks," *Pattern Recognit.*, vol. 77, pp. 354–377, 2018.
[38] X. Liu, C. Deng, J. Chanussot, D. Hong, and B. Zhao, "Stfnet: A two-stream convolutional neural network for spatiotemporal image fusion," *IEEE Trans. Geosci. Remote Sens.*, vol. 57, no. 9, pp. 6552–6564, Sep. 2019.
[39] W. Song, S. Li, L. Fang, and T. Lu, "Hyperspectral image classification with deep feature fusion network," *IEEE Trans. Geosci. Remote Sens.*, vol. 56, no. 6, pp. 3173–3184, Jun. 2018.
[40] B. Xu, N. Wang, T. Chen, and M. Li, "Empirical evaluation of rectified activations in convolutional network," 2015, *arXiv:1505.00853*.
[41] Q. Yin, J. Li, Y. Zhou, D. Xiang, and F. Zhang, "Adaptive weighted learning for vegetation contribution in soil moisture inversion using PolSAR data," *Int. J. Remote Sens.*, vol. 43, no. 9, pp. 3190–3215, 2022.
[42] W.-C. Tseng, "Weichengtseng/pytorch-pcgrad," 2020. [Online]. Available: https://github.com/WeiChengTseng/Pytorch-PCGrad.git
[43] T. Yu, S. Kumar, A. Gupta, S. Levine, K. Hausman, and C. Finn, "Gradient surgery for multi-task learning," in *Proc. 34th Int. Conf. Neural Inf. Process. Syst.*, 2020, vol. 33, pp. 5824–5836.
[44] M. Williams, "Prediction and observation of SAR clutter from vegetation canopies," in *Proc. IEEE Int. Geosci. Remote Sens. Symp.*, 1999, pp. 1983–1985.
[45] F. Xue, X. Wang, F. Xu, and Y. Wang, "Polarimetric SAR interferometry: A tutorial for analyzing system parameters," *IEEE Geosci. Remote Sens. Mag.*, vol. 8, no. 2, pp. 83–107, 2020.
[46] E. Pottier and L. Ferro-Famil, "Polsarpro v5. 0: An ESA educational toolbox used for self-education in the field of PolSAR and Pol-InSAR data analysis," in *Proc. IEEE Int. Geosci. Remote Sens. Symp.*, 2012, pp. 7377–7380.
[47] T. Fatoyinbo et al., "The NASA AfriSAR campaign: Airborne SAR and LiDAR measurements of tropical forest structure and biomass in support of future space missions," *Authorea Preprints*, vol. 264, 2022, Art. no. 112533.
[48] J. Armston et al., "Afrisar: Gridded forest biomass and canopy metrics derived from LVIS, Gabon, 2016," ORNL DAAC, Oak Ridge, TN, USA, 2020.
[49] M. Denbina and M. Simard, "Kapok: An open source Python library for PolinSAR forest height estimation using UAVSAR data," in *Proc. IEEE Int. Geosci. Remote Sens. Symp.*, 2017, pp. 4314–4317.
[50] V. Wasik, P. C. Dubois-Fernandez, C. Taillandier, and S. S. Saatchi, "The AfriSAR campaign: Tomographic analysis with phase-screen correction for P-band acquisitions," *IEEE J. Sel. Topics Appl. Earth Observ. Remote Sens.*, vol. 11, no. 10, pp. 3492–3504, Oct. 2018.
[51] A. G. Fore et al., "UAVSAR polarimetric calibration," *IEEE Trans. Geosci. Remote Sens.*, vol. 53, no. 6, pp. 3481–3491, Jun. 2015.

Dandan Li is currently working toward the Ph.D. degree in forestry engineering with Northeastern Forestry University, Harbin, China.

Her research interests and expertise include remote sensing and SAR.

Hailiang Lu received the B.E. degree in computer science and technology and M.A. degree from Inner Mongolia Agricultural University, Hohhot, China, in 2018 and 2020, respectively. He is currently working toward the doctorate degree with Northeast Forestry University, Harbin, China.

His research interests include deep learning and intelligent interpretation of remote sensing images.

Chao Li received the Ph.D. degree in information and communication systems from the Harbin Institute of Technology, Harbin, China, in 2012.

She is currently the Deputy Director of artificial intelligence and master's Tutor with Harbin Northeast Forestry University, Harbin, China. She was a Visiting Scholar with the Center for Forestry and Natural Resources, University of West Virginia, Morgantown, WV, USA. She has chaired and completed projects, such as the National Natural Science Foundation of China Youth Project. She has authored or coauthored more than 20 SCI/EI retrieval papers with the first author and corresponding author. Her research interests include signal processing, feature extraction, and multimodal fusion.

Dr. Li is also the Member of the China Computer Federation and the Chinese Society of Forestry. She was the recipient of the second Prize in Heilongjiang Provincial Science and Technology Progress Award.

Linda Mohaisen received the B.S. degree in computer science from King Abdul Aziz University, Jeddah, Saudi Arabia, in 2004, the M.S. degree in computer engineering from the University of Central Florida, Orlando, FL, USA, in 2011, and the Ph.D. degree in artificial intelligence from the University of Alabama in Huntsville, Huntsville, AL, USA, in 2018.

She is currently with the Faculty of Computing and Information Technology, King Abdul Aziz University, Jeddah, Saudi Arabia. She has authored and coauthored of some publications and a referee of many referred international journals and conferences. Her research interests include artificial intelligence, wireless communication, mobile network, vehicular ad hoc network, wireless sensor network, hybrid network, cross-layer design, and modeling and performance evaluation of computer networks.

Weipeng Jing (Member, IEEE) received the Ph.D. degree in computer architecture from the Harbin Institute of Technology, Harbin, China, in 2016.

He is currently a Professor with Northeast Forestry University, Harbin, China. He has authored or coauthored more than 100 research articles in refereed journals and conference proceedings. His research interests include modeling and scheduling for distributed computing systems, Artificial intelligence, and spatial data mining.

He was the Publication Chair of International Conference of Pioneering Computer Scientists, Engineers and Educators in 2016–2020, National Conference on Big Data Technology and Applications in 2017 and 2015, Collaborate 2017, Annual International Conference on Wireless Internet 2016, and International Conference on Future Internet of Things and Cloud 2016. Dr. Jing is also the Member of ACM and a Senior Member of the China Computer Federation.